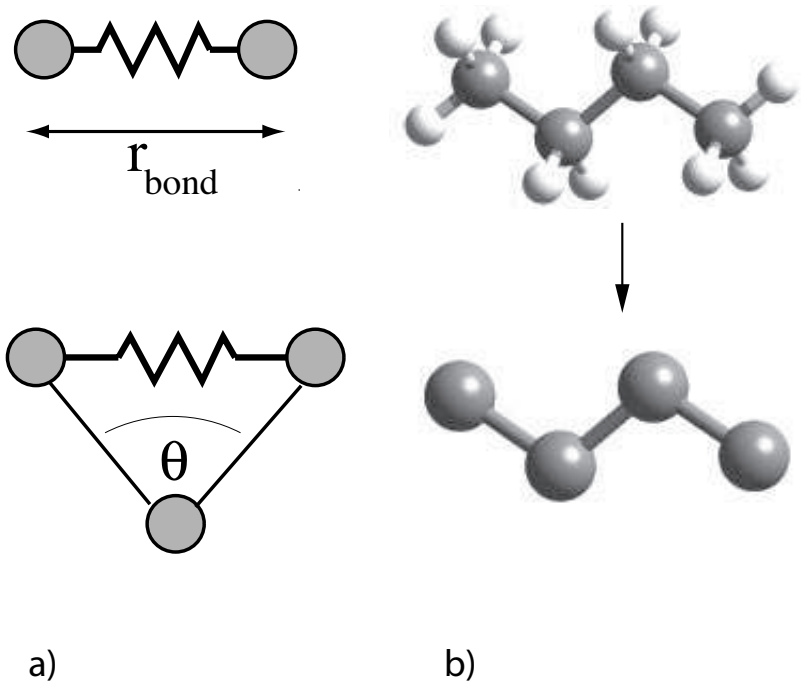

Figure 2.29: The bond potentials

sub-indices mark the positions in the chain: 0 and $N+1$ are the end points of the chain and the numbers between them denote the linking points of rods in the chain.

The bonded interactions between neighboring units are given by harmonic length and angle potentials:

$$H_{bond} = \frac{1}{2}k(r-r_0)^2 \tag{2.129}$$

$$H_{angle} = \frac{1}{2}k_\theta(\cos\theta - \cos\theta_0)^2 \tag{2.130}$$

with the bond lengths r and the bending angles θ. Here r_0 and θ_0 denote the mean values.

2.1.7 Macromolecules in solution

Important Concepts: Flory-Huggins theory, θ-temperature, phase transitions, morphology, nucleation, spinodal decomposition

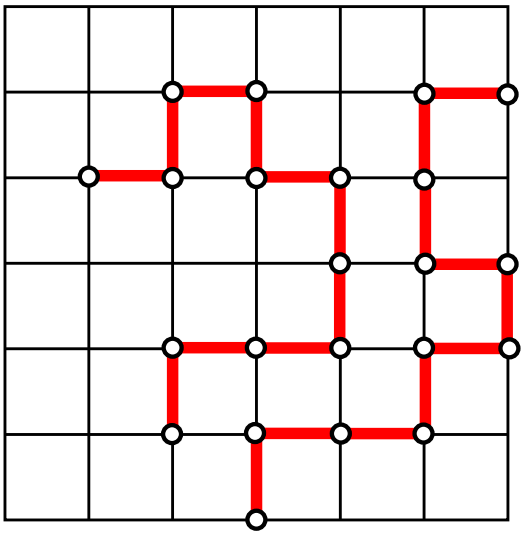

Figure 2.30: Lattice statistics for polymers as considered in the Flory-theory

The *Flory-Huggins theory* of polymer solutions is based on a lattice theory. It is a mean-field theory.

Macromolecules occupy 30 percent of the volume of the cell, strongly influencing inter-molecular interactions. The density of the molecules causes like species to phase separate into different regions of the cell, leading to *macromolecular compartmentalization* .

We consider a solution of solvent molecules and polymers (see figure **??**). For simplicity we assume that the monomers of the polymer with length N have the same size as the solvent molecules. We further simplify by constraining the polymers and the solvent molecules to be on a lattice. This gives us the possibility to count the number of putting a polymer at n lattice sites with coordination number q. Let N_1 be the number of solvent molecules and N_2 be the number of polymers ($n = N_1 + NN_2$).

We assume that the polymer molecules are numbered and are placed on the lattice one after the other according to their numbers. If the number of possible ways to place the i-th monomer after the one has placed the first $i-1$ polymer is called ν_i, then the number of ways to place all the other polymers on the lattice is given by $\nu_1, \nu_2, ...\nu_{N_2}$. Since we cannot distinguish the polymer monomers, we must have

$$W = \frac{1}{N_2!} \prod_{i=1}^{N_2} \nu_i \tag{2.131}$$

for the number of configurations. Next we need to approximate ν_i. We have numbered the monomers along the chain by $1, 2, 3, ..., N$. We place the monomers on the lattice according to their ordering. The first monomer can be placed anywhere on a free lattice site. The number of possible ways to do this is

$$n - N(i-1) \tag{2.132}$$

The second monomer needs to be placed on one of the q nearest-neighbours. We make the approximation that one can replace the probability of finding a neighbour site occupied by the polymers one has already placed by the probability one would have if all other monomers were distributed randomly over the lattice. From this assumption one obtains

$$q[1 - N(i-1)/n] \tag{2.133}$$

for the number of ways for doing so. The third monomer needs to be placed to a nearest-neighbour site to the second monomer. One of the neighbour sites has already been taken therefore we get

$$(q-1)[1 - N(i-1)/n] \tag{2.134}$$

for the third monomer. If we neglect the possibility that the fourth monomer happens to be placed next to the first monomer we find the same situation for the fourth as for the third monomer. Let σ be the symmetry number of the polymer which is 2 for a polymer which is symmetric with respect to the center and 1 otherwise. Then we have

$$\nu_i = \frac{n}{\sigma} q (q-1)^{N-2} \left[1 - \frac{N(i-1)}{n}\right]^N \quad , \tag{2.135}$$

because it does not matter from which end we start laying down the polymer on the lattice. Substituting this expression into **??** we obtain

$$W = \frac{q^{N_2}(q-1)^{N_2(N-2)}}{N_2!\sigma^{N_2}} n^{N_2} \prod_{i=1}^{N_2} \left[1 - \frac{N(i-1)}{n}\right]^N \quad (2.136)$$

$$= \frac{q^{N_2}(q-1)^{N_2(N-2)}}{N_2!\sigma^{N_2}} n^{-(N-1)N_2} \left[N^{N_2} \frac{(n/N)!}{(N_1/N)!}\right]^N \quad . \quad (2.137)$$

The vacant sites must be filled with the solvent. Hence the whole solution is determined by the configuration of the polymers and also the entropy of the solution is given by

$$S = k_B \ln W \quad . \quad (2.138)$$

Inserting **??** into this we get

$$S(N_1, N_2) = N_2 k_B \ln \frac{q(q-1)^{N-2}}{\sigma e^{N-1}} - k_B \left[N_1 \ln \frac{N_1}{n} + N_2 \ln \frac{N_2}{n}\right] \quad . \quad (2.139)$$

We can obtain this result from a purely thermodynamic consideration. Assume that we have two species each obeying the ideal gas law. The gases are in a container speparted by a wall. We first expand one of the gases isothermally

$$dU = Tds - pdV \quad (2.140)$$

Hence

$$Tds = pdV \quad (2.141)$$

$$dS = \frac{nR}{V} dV \quad (2.142)$$

which gives

$$\Delta S_1 = n_1 R \ln \frac{V_1 + V_2}{V_1} \quad . \quad (2.143)$$

For the second gas we find

$$\Delta S_2 = n_2 R \ln \frac{V_1 + V_2}{V_2} \quad (2.144)$$

So that in total we get

$$\Delta S = \Delta S_1 + \Delta S_2 = n_1 R \ln \frac{V_1 + V_2}{V_1} + n_2 R \ln \frac{V_1 + V_2}{V_2} \quad (2.145)$$

$$= -R \left(n_1 \ln \frac{V_1}{V_1 + v_2} + n_2 \ln \frac{V_2}{V_1 + v_2} \right) \quad (2.146)$$

The model has some restrictions. First, there is no change of volume during mixing. Second, the entropy of mixing is entirely given by the number of rearrangements during mixing. The enthalpy of mixing is caused by interactions of different segments after the dissolution of interactions of the same type of segments.
We shall assume that there is random mixing of two polymers with no volume change. Then the combinatorial entropy of mixing is given by

$$\Delta S = -R \left(\frac{c_1}{N_1} \ln c_1 + \frac{c_2}{N_2} \ln c_2 \right) \quad (2.147)$$

with c_i being the volume fraction of the component i and N_i the number of monomers. Here R is the gas constant.
If we assume the concept of regular solutions and assuming pair interactions then, in the framework of a mean-field theory, we obtain for the enthalpy of mixing

$$\Delta H = RT \chi c_1 c_2 \quad . \quad (2.148)$$

Here χ is the Flory-Huggins parameter assumed not to be a function of the composition. The Flory-Huggins equation is now given by

$$\Delta S = -RT \left(\frac{c_1}{N_1} \ln c_1 + \frac{c_2}{N_2} \ln c_2 + \chi c_1 c_2 \right) \quad . \quad (2.149)$$

Before we continue to examine the free energy we shall first look at model for the internal energy. Let $n = N_1 + N_2$, i.e. we consider monomers at the moment. We introduce concentrations for the cell for the two species, solvent molecules and nomomers c_i^1 and c_i^2 in the i-th cell. Since

$$c_i^2 = 1 - c_i^1 \quad (2.150)$$

we can introduce $c_i \equiv c_i^1$ with

$$N_1 = \sum_{i=1}^{n} c_i \quad , N_2 = \sum_{i=1}^{n} (1 - c_i) \quad . \tag{2.151}$$

With these we can write down an interaction Hamiltonian

$$\begin{aligned} H(\{c_i\}) &= \sum_{\mu,\nu=1,2} \sum_{i,j} V_{i,j}^{\mu\nu} c_i^{\mu} c_j^{\nu} && (2.152) \\ &= \sum_{i,j} \left\{ V_{ij}^{11} c_i c_j + V_{ij}^{22} (1 - c_i)(1 - c_j) + 2 V_{ij}^{12} c_i (1 - c_j) \right\} && (2.153) \end{aligned}$$

Let

$$s_i = \begin{cases} +1 & \text{if cell } i \text{ is occupied by a solvent molecule} \\ -1 & \text{if cell } i \text{ is occupied by a solute molecule} \end{cases} \tag{2.154}$$

then the above Hamiltonian reduces to the Ising model, if we let

$$\begin{aligned} J_{ij} &\equiv V_{ij}^{12} - \frac{1}{2}(V_{ij}^{11} + V_{ij}^{22}) && (2.155) \\ V^{\mu\nu} &\equiv \sum_j V_{j1}^{\mu\nu} && (2.156) \\ J &\equiv \sum_j J_{j1} && (2.157) \end{aligned}$$

and hence

$$H(\{c_i\}) = -\frac{1}{2} \sum_{ij} J_{ij} s_i s_j + \frac{V^{11} - V^{22}}{2} + \frac{n}{2} J \quad . \tag{2.158}$$

It follows that the internal energy within this model is given by

$$U/n = -2J \left(c - \frac{1}{2} \right)^2 + Kc + \text{const} \tag{2.159}$$

with the segment concentration

$$c = \frac{N \cdot N_2}{n} \quad . \tag{2.160}$$

With eqs **??** and **??** we obtain for the free energy

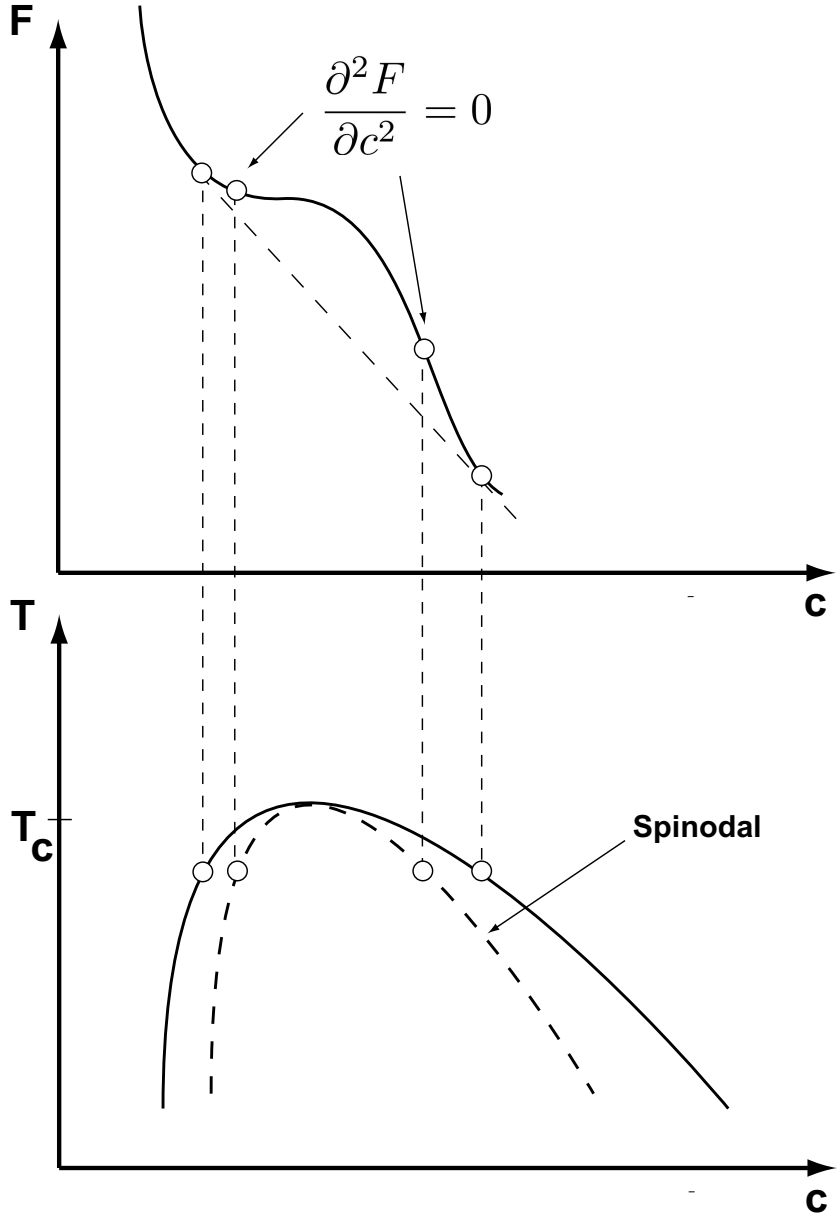

Figure 2.31: Free energy and phase diagram for macromolecular solutions

$$F/n = -2J\left(c-\frac{1}{2}\right)^2 + T\left\{\frac{c}{N}\ln\frac{c}{N} + (1-c)\ln(1-c) - \chi\frac{c}{N} + \text{const}\right\} \tag{2.161}$$

Figure **??** shows the free energy and the resulting phase diagram. For large values of T only one minimum exists irrespective of the concentration. The system will be in the one-phase region. For low temperatures we get a situation as shown in figure **??**. Note that the free energy has two inflection points defining spinodal points by the condition

$$\frac{\partial^2 F}{\partial c^2} = 0 \tag{2.162}$$

and hence

$$\frac{4J}{T} = \frac{1}{Nc} + \frac{1}{1-c} \quad . \tag{2.163}$$

The states within these inflection points are unstable, while the states between the *coexistence curve* (also called *binodal*) are *metatstable*. The spinodal touches the binodal at the critical point. For the *critical concentration* we obtain

$$0 = -\frac{1}{Nc^2} + \frac{1}{(1-c)^2} \tag{2.164}$$

and hence

$$c_{\text{crit}} = \left(1+N^{-1/2}\right)^{-1} \quad . \tag{2.165}$$

For the *critical temperature* we obtain

$$T_c^{\text{MF}} = \frac{4J}{1+2N^{1/2}+N^{-1}} \quad , \tag{2.166}$$

where the superscript indicates that we have obtained the result within a mean-field theory. As $N \to \infty$ we find

$$T_c^{\text{MF}} \to 4J \tag{2.167}$$

and

$$c_{\text{crit}} = 0 \quad . \tag{2.168}$$

To understand this point better we consider the *osmotic pressure* describing the tendency of the polymers to disperse in the solution

$$\Pi = -\frac{\partial}{\partial V}[F(c) - F(0)]|_{NN_2=\text{fixed}} \tag{2.169}$$

Since $V = n$ (the cell volume = 1) we have

$$\begin{aligned} -\Pi &= \frac{\partial(\Delta F)}{\partial n}|_{N=\text{fixed}} && (2.170)\\ &= \frac{\partial}{\partial 1/c}\left(\frac{\Delta F}{N}\right)|_{N=\text{fixed}} && (2.171)\\ &= -c^2\frac{\partial}{\partial c}\left(\frac{\Delta F}{n}\right) && (2.172) \end{aligned}$$

Substituting eq **??** for F we find

$$\Pi = -2Jc^2 + T\left\{\frac{c}{N} - c - \ln(1-c)\right\} \quad . \tag{2.173}$$

For $c \ll 1$ we get

$$\Pi = T\frac{c}{N} + \left(\frac{T}{2} - 2J\right)c^2 + O(c^3) \quad . \tag{2.174}$$

The first term is the ideal gas result and the second term is the second virial coefficient. J is thus the effective attraction between polymers. For $T = 4J$ we have the ideal gas result even for large c singling out this temperature as the $theta$-*temperature* (see figure **??**).
In the region where $c/N \ll c^2$ the macromolecules will be well separated (ideal gas). For $c^* = 1/N$ we will have the beginning of the overlap of macromolecules. In the concentration region

$$c^* \ll c \ll 1 \tag{2.175}$$

we find

$$\Pi \approx c^2 \quad . \tag{2.176}$$

We can now define the temperature, where the second virial coefficient vanishes as the θ-*temperature*. Below this temperature the chain shows the statistics of a

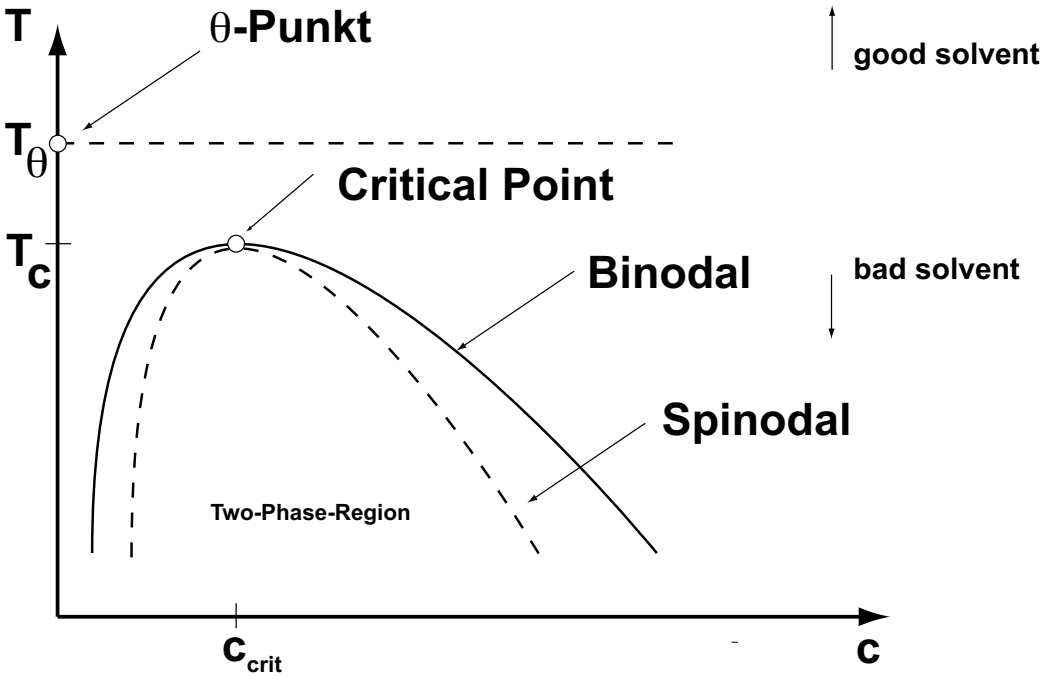

Figure 2.32: Phase diagram for macromolecular solutions

self-avoiding random walk. Above the chain conformations can be statistically considered as those of a random walk.
Flory Huggins free energy

$$F = \int dV \left[\phi \ln \phi + (1-\phi)\ln(1-\phi) + \xi\phi(1-\phi) + \frac{\kappa}{2}(\nabla\phi)^2\right] \qquad (2.177)$$

2.1.8 Macromolecules at surfaces

By special endgroups flexible macromolecules can be tethered to a substrate via its chain end. Polymers can be grafted or brought close to a hard wall as well as to a number of soft interfaces. These include surfactant or phospholipid bilayers in cells, in vesicles and in other membrane solutions [**?**]. Very interesting is the case of biological grafting. There, phospholipid bilayers build the walls of liposomes and cells, hosting proteins responsible for functions as diverse as anchoring the cytoskeleton [**?**]. When a polymer is grafted to a bilayer it can induce gelation [**?**]

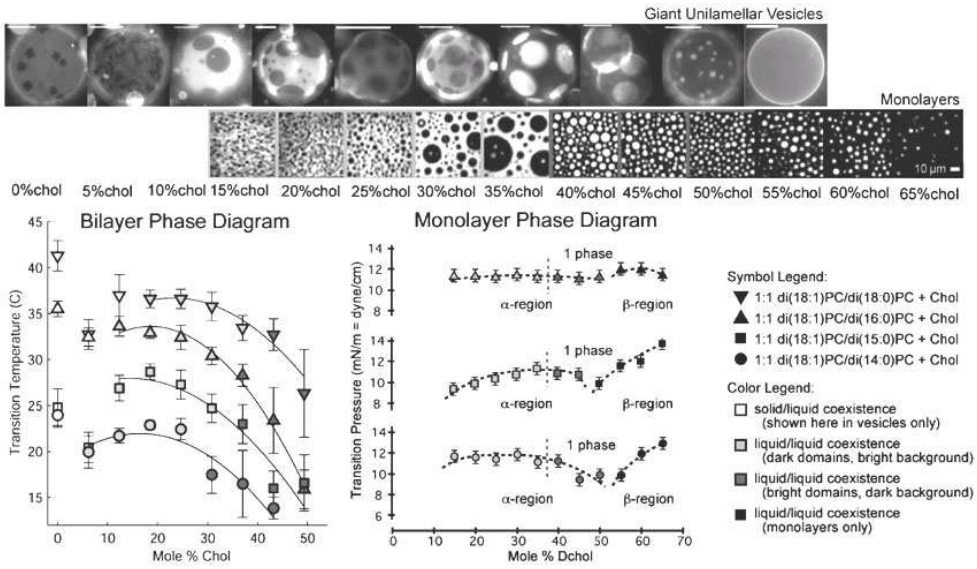

Figure 2.33: (top) A series of fluorescence micrographs of vesicles and monolayers of 1:1 di(18:1)PC / di(16:0)PC with varying cholesterol. Scale-bars are 20μm for vesicles and 10μm for monolayers. From left to right, the phases are solid-liquid coexistence, coexisting liquid phases, and either one uniform liquid phase (in vesicles), or coexisting liquid phases (in monolayers). (bottom left) Miscibility transition temperatures for vesicles. Points at low cholesterol represent melting of the solid phase. Filled points mark miscibility transi- tion temperatures for two liquid phases. Temperatures from 10C-50C are experimentally accessible. Error bars represent standard deviations over multiple measurements. (bottom right) Miscibility transition surface pressures for monolayers. The change of contrast is marked by a vertical gray dashed line. For all domains $\geq$10μm, striping of domains was seen near the transition. Striping may occur in smaller domains beyond our resolution. In all cases, curves are drawn to guide the eye and are not explicit fits of the data. (taken from the PhD-thesis *Liquid Immiscibility in Model Bilayer Lipid Membranes* by Sarah L. Veatch, University of Washington, 2004)

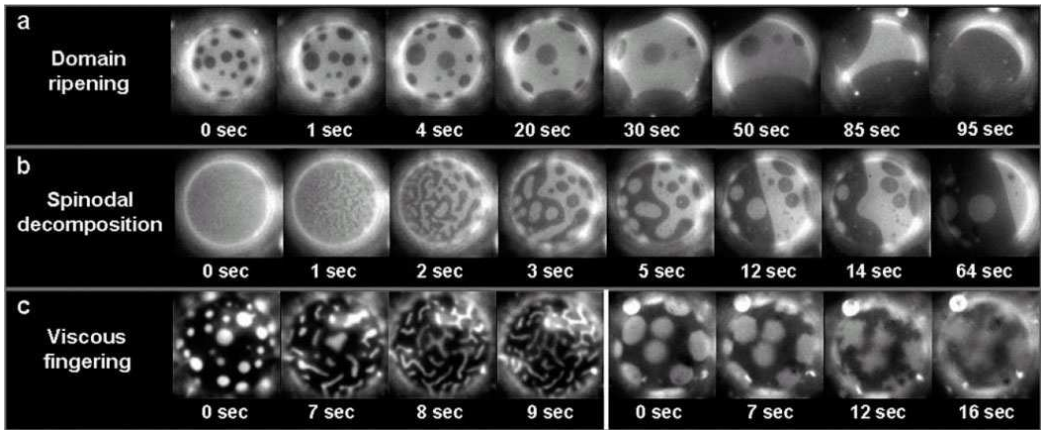

Figure 2.34: Giant vesicles observed near the miscibility transition. (a) Domain ripening through time in a vesicle of 1:1 DOPC/DPPC + 25 % Chol. Although the proportion of dark phase increases in one hemisphere, it is roughly constant in time over the entire vesicle. (b) Time sequence suggesting spinodal decomposition in a vesicle of 1:1 DOPC/DPPC + 35% Chol. (c) Viscous fingering in a vesicle of 1:9 DOPC/DPPC + 25% Chol (left series) and 1:1 DOPC/DMPC + 25% Chol (right series) as temperature is raised through the miscibility transition. The uniform stripe-widths shown at the left is unique to this vesicle composition. All vesicles are roughly 30μm in diameter. (taken from the PhD-thesis *Liquid Immiscibility in Model Bilayer Lipid Membranes* by Sarah L. Veatch, University of Washington, 2004)

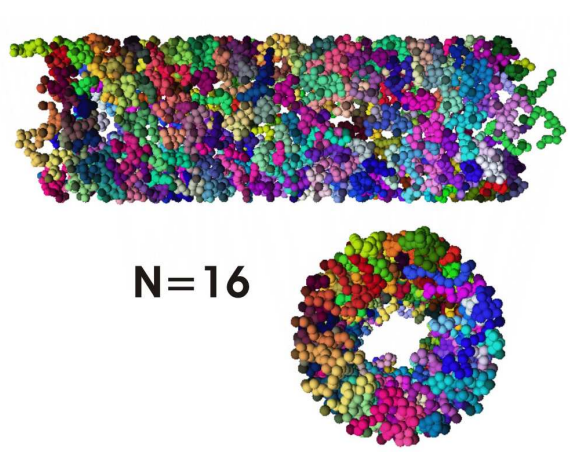

Figure 2.35: Snapshot picture of a brush grafted inside of a cylinder, for $N = 16$, $D = 30, \sigma = 0.08$, displaying different chains in distinct colors in order to be able to distinguish them. Top shows a side view of the cylinder, lower part a view of the cross section. Note that the particles forming the cylindrical wall are not displayed.

or other phase changes [**?**, **?**] in liquid lamellar phases. They can also stabilize monodisperse vesicles [**?**].

When a polymer chain is brought in the neighbourhood of a repulsive, impenetrable wall, the number of conformations available to the chain is reduced [**?**, **?**]. The average configuration of the polymer is a compromise between the need to avoid the wall and the constraint imposed by the grafted end of the chain. Thus the statistics of conformations will be influenced. In a dilute solution under good solvent conditions using a non-adsorbing substrate surface that repels the monomers one thus obtains a "mushroom" configuration of the polymer [**?**, **?**]. If one grafts many such polymer chains on the substrate, such that the polymer coils in their mushroom configuration would strongly overlap each other, excluded volume interactions reduce this overlap by leading to strongly stretched configurations of the coils, the so-called "polymer brushes" [**?**, **?**]. In this way, the substrate is coated with a polymeric layer of height h proportional to the chain length N of these endgrafted polymers [**?**, **?**, **?**, **?**].

For brushes on flat substrates one has the well known property $h \propto N$ for large enough N. For brushes on cylindrical substrates with small enough D the brushes

are compressed and hence a weaker increase is expected. However, one expects from the self-consistent field theory that for not too large N (or large enough D, respectively, such that the center of the cylinder is still more or less free of monomers, cf. Fig **??**) that the density profile of a brush decreases somewhat slower in a cylindrical brush than for the corresponding blobs in a brush on the flat substrate, under identical conditions. For the "blobs" close to the cylinder axis, less volume is available than for corresponding blobs in a brush on a flat substrate. As a consequence, a correspondingly stronger stretching tendency for chains in a blob grafted to the inner surface of the cylinder would be predicted. Our numerical results for brushes in cylinders with large enough D (Fig. **??**) are comparable with this prediction. Hence, the theoretical result of Sevick [**?**] that the brush height is longest for $D \to \infty$ and decreases monotonously while decreasing D is not confirmed by our simulations. Of course, this trend seen on Fig. **??** cannot hold indefinitely with increasing N. When all the free volume in the center of the brush (Fig. **??**) is filled up with monomers, compression of the brush sets in, and consequently the monomer density gets enhanced also in the region of the brush close to the cylinder walls. In this regime, we expect that the height of a brush on a flat substrate would be larger than the height of the brush, confined into the cylinder, and this is nicely demonstrated for a narrow enough tube in Fig. **??** too.

We consider the pressure that a grafted chain exerts on a wall. Consider a wall with a repulsive r^6 potential an a polymer grafted at the wall. The constraint, that the polymer is grafted and that one half-space is excluded leads to a competition between the necessity to avoid the wall and the constraint to be fixed at the wall. Because of entropic reason the monomers would like to stay as far away from the wall as possible. In order to do so they exert a pressure on the wall [**?**, **?**]. This pressure decreases radially from the grafting point.

Following **??**, let $h(x, y)$ be the height distribution on the wall. The thermodynamic properties of the chain of length N grafted at the repulsive wall can be described by the propagator $G_N(\vec{r}, \vec{r}')$ resulting from the Edwards equation

$$\frac{\partial G_N(\vec{r}, \vec{r}')}{\partial N} = \frac{l^2}{6} \Delta G_N(\vec{r}, \vec{r}') \tag{2.178}$$

with the $G_N(\vec{r}, \vec{r}') = 0$ at the wall and $\lim_{N \to 0} G_N(\vec{r}, \vec{r}') = \delta(\vec{r}, \vec{r}')$. The partition sum is then given by

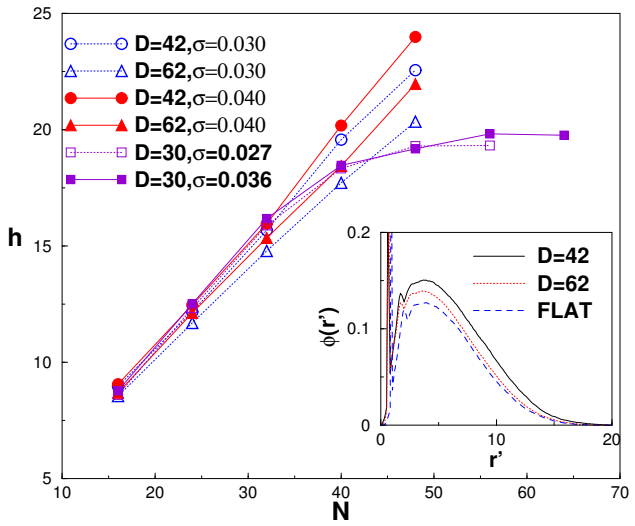

Figure 2.36: Brush height h plotted vs N for various diameters D and grafting densities σ, as indicated. Insert compares the density profiles $\phi(r')$ vs. r' for two choices of D at $\sigma = 0.03$ with the monomer density profile of a flat brush.

$$Z_N(l) = \int d\vec{r}' G_N(\vec{r}, \vec{r}') \tag{2.179}$$

where the integral extends over all space that is available to the free end. The Greens-function for $h(x, y) = 0$ can be factorized as

$$G_N^{(0)}(\vec{r}, \vec{r}') = \left(\frac{3}{2\pi N l^2}\right)^{3/2} \exp\left[-\frac{3(x-x')^2}{2Nl^2}\right] \exp\left[-\frac{3(y-y')^2}{2Nl^2}\right] \times \left(\exp\left[-\frac{3(z-z')^2}{2Nl^2}\right] - \exp\left[-\frac{3(z+z')^2}{2Nl^2}\right]\right) .$$

The partition function is

$$Z_N^{(0)}(l) = \int_{-\infty}^{+\infty} dx' \int_{-\infty}^{+\infty} dy' \int_0^{+\infty} dz' G_N^{(0)}(\vec{l}, \vec{r}') \tag{2.180}$$

$$= \mathrm{erf}(\frac{l}{2R_g}) \tag{2.181}$$

where $R_g = \sqrt{Nl^2/6}$ the radius of gyration of the free chain and erf the error function. To compute the pressure we introduce a small perturbation in h. We can write the partition function as $Z_N = Z_N^{(0)} + Z_N^{(1)} + Z_N^{(2)} + \ldots$, where $Z_N^{(i)}$ is of order h^i and Z_N^0 as in(**??**). Because of the linearity of (**??**), each terms satisfies the Edwards equation

$$\frac{\partial Z_N^{(i)}}{\partial N} = \frac{l^2}{6}\Delta Z_N^{(i)} \quad i = 0, 1, 2, \ldots \tag{2.182}$$

The solution of higher order are coupled to the constraint. Now we have

$$\begin{aligned} 0 &= Z_N(x, y, h) \\ &= Z_N(x, y, 0) + h(x, y)\frac{\partial Z_N}{\partial z}(x, y, 0) + \frac{h^2(x, y)}{2}\frac{\partial^2 Z_N}{\partial z^2}(x, y, 0) + \ldots \end{aligned}$$

For the linear contribution $Z_N^{(1)}$ we get

$$Z_N^{(1)}(x, y, 0) = -h(x, y)\frac{\partial Z_N^{(0)}}{\partial z}(x, y, 0) \tag{2.183}$$

yielding [**?**]

$$Z_N^{(1)}(\vec{l}) = \frac{l^2}{6}\int_0^N dn \int dS \frac{\partial G_{N-n}^0}{\partial z}(x, y, 0; \vec{a}) Z_n^{(1)}(x, y, 0) \tag{2.184}$$

Hence, the change in the height is, to first order, due to the work

$$\begin{aligned} \Delta W &= W[h] - W[0] \\ &= -k_B T \log\left[1 + \frac{Z_N^1}{Z_N^0}\right] \\ &= \int dS p(x, y) h(x, y) \end{aligned}$$

where $p(x, y)$ has the symmetric form

$$p(r) = \frac{k_B T}{2\pi(r^2 + l^2)^{3/2}}\left(1 + \frac{r^2 + l^2}{2R_g^2}\right)\exp\left[-\frac{r^2 + l^2}{4R_g}\right] \quad , \tag{2.185}$$

with $r = \sqrt{x^2 + y^2}$. To push at $\vec{r} = (x, y)$ an elementary volume of $dV(r) = h(r)dS$ we need the work $dW = p(r)h(r)dS$. The function $p(r)$ is the pressure. The entire entropic force which the chain exerts on the wall is then given by

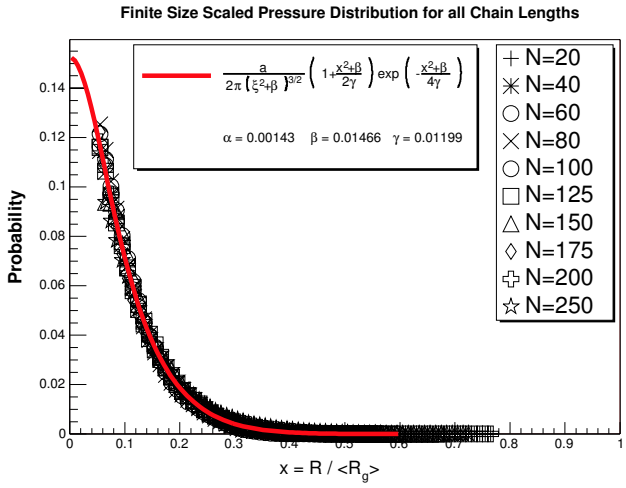

Figure 2.37: Finite-size scaling plot for the pressure distribution. The full curve is the fit using the predicted form of the distribution. The fit is very good over the entire region.

$$F = \int_0^\infty dr 2\pi r p(r) = \frac{k_B T}{l} \exp\left[-\frac{l^2}{4R_g^2}\right] \tag{2.186}$$

$$= \frac{k_B T}{l} \exp\left[-\frac{3}{2N}\right] \quad . \tag{2.187}$$

We have simulated 10 different chain lengths $N = 20, N = 40, N = 60, N = 80, N = 100, N = 125, N = 150, N = 175, N = 200$ and $N = 250$ to study the pressure and the corresponding finite effects.

In Figure**??** we show the finite-size scaling plot for the pressure distribution. The full curve is the fit using the predicted form of the distribution (see **??**). The fit is very good over the entire region.

In Figure **??** is shown the entropic force exerted on the wall by the polymer. The figures gives the result for the gaussian and for the chain with self-avoidance.

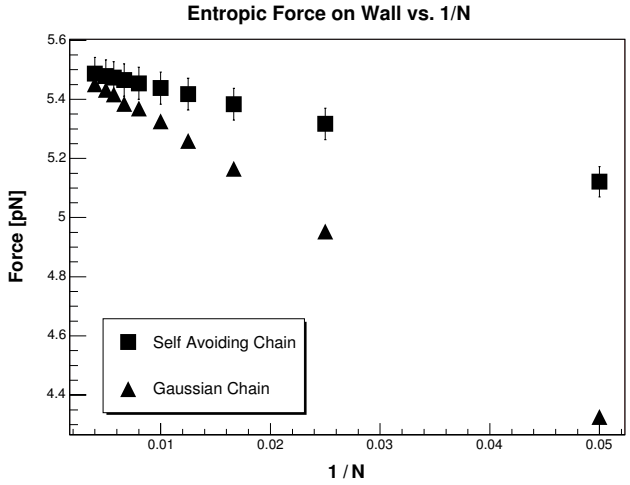

Figure 2.38: Shown is the entropic force exerted on the wall by the polymer. The figures gives the result for the gaussian and for the chain with self-avoidance.

2.2 Intermolecular interactions and electrostatic screening

The total potential energy of a single macromolecule can be divided into bonding and non-bonding parts. The bonding energies are due to the local covalent bonds. We shall now focus on the non-bonding part.
Charged polymers are essential for biology. Many functions depend critically on the activity of DNA, RNA and proteins all of which are charged polymers. A human nuclear DNA molecule carries hundreds of millions of charged groups. Inseparable from the polymer phenomenology is the behavior of the small charged mobile anions which dissociate from their backbones and interact strongly with the polymer chains.
Interactions between charges relevant in biology are almost always affected by the presence of water molecules, ions, and other molecules. The interactions are reduced in strength or are screened.
Non-covalent interactions are much weaker than the covalent bonds. We classify the non-covalent interactions in (decreasing in strength)

- Ionic interactions

- Intermediate dipole-dipole forces
- Hydrogen bonds
- Hydrophobic interactions
- Van der Waals interactions: The force arises from induced dipole and the interaction is weaker than the dipole-dipole interaction.
- **Ionic interactions**

  Let us first discuss the ionic interactions. What we always have to consider is water. Pure H_2O has pH 7.0. Hence even pure water is not the simple dielectric.

  Many proteins, nucleic acids, and other organic molecules in cells are charged. They give up ions to the solution when they are put in water. A good example is DNA, which has one phosphate ion (PO_4-) on each nucleotide. The anion is usually Na^+.

  Important functional ionic groups are for the anionic case

  - carboxy
  - sulfate
  - sulfonate
  - phosphate

  and for the cationic case

  - amino
  - imimo
  - ammonium
  - sulfonium
  - phosphonium

  On a more detailed scale biologically the following ions are of interest:

- **Univalent ions**. The cations Na^+ and K^+ are present at roughly 0.1 M concentrations, outside and inside cells, respectively. There are anions (negative ions) at the same concentration to balance the charge.
- **Divalent ions** Charge-2 cations like Mg^2+ and Ca^2+ are present at roughly mM concentrations in cells, and in many biochemistry experiments.

Let q_1 and q_2 be two charges. Then the potential is given by

$$U(r) = \frac{kq_1q_2}{r} \tag{2.188}$$

with $k = 8.99 \times 10^9 N\Delta m^2/C^2$ in vacuum.

Table 2.3: Potential for two charges separated a distance of about 2nm at room temperature

vacuum	$30k_BT$
water	$0.4k_BT$

The charges, which are embedded in a dielectric material (water) interact by a Coulomb interaction which is reduced in strength measured by the dielectric constant. Water molecules have a very large electric dipole moment and are forced to rotate to respond to an alternate external electric field. Hence water as a liquid has a very large dielectric constant 80 at room temperature. This reduction in strength of the Coulomb interaction is due to the polarization of the particles of the dielectric medium - either induced or permanent dipoles around a free charge will be oriented so as to terminate some of the field lines coming from the free charge. The Coulomb interaction continues to have its long-ranged character, just with a reduced strength (dielectric screening of the charge).

$$\lambda_D = \sqrt{\frac{\epsilon_0\epsilon_r k_BT}{2N_Ae^2I}} \tag{2.189}$$

where ϵ_0 is the permittivity of free space.

The *Bjerrum length* l_B is the distance at which the Coulomb interaction between two unscreened charges equals the thermal energy

$$l_B = \frac{e^2}{4\pi\epsilon\epsilon_0 k_B T} \tag{2.190}$$

Example 2.2.1
The Bjerrum length at which two electron charges have an interaction energy about $k_B T$ in pure water at standard pressure and temperature is 0.7 nm where we have used

$$\begin{aligned} k &= 9 \times 10^9 N\Delta m^2/C^2 && (2.191)\\ e &= 1.6 \times 10^{-19}\, C && (2.192)\\ e &= 80 && (2.193)\\ k_B T &= 4 \times 10^{-21}\, J && (2.194) \end{aligned}$$

There is another very important screening effect that arises from free ions in solution and which will cluster around charged objects, counter-ions and further reduces the strength and range of the Coulomb interactions. These counter-ions can be associated with the charged objects with energies in excess of $5k_B T$ and hence are not easily shaken off by thermal energy.

- **Charge-dipole and dipole-dipole interactions**

  Many molecules are electrically neutral but have a permanent dipole because of an asymmetric distribution of the electron cloud around the positively charged nuclei. For example, in HCl, the valence electron of the H atom is donated to the Cl atom, with H carrying a net positive charge, and Cl a net negative charge. Similarly, water has a permanent dipole because the electron density is greater near the more electro negative O atom.

  Recall that the *dipole moment* is defined as $|\mathbf{q}| = qd$ where d is the separation between 2 charges $+q$ and $-q$. $\mathbf{p}$ is a vector and points in the direction from $-q$ to $+q$. When a molecule with a dipole moment $\mathbf{p}$ is placed in an electric field $\mathbf{E}$, the dipole has a potential energy

$$U(\theta) = \mathbf{p} \cdot \mathbf{E} = -pE\cos\theta \quad . \tag{2.195}$$

– **Charge-dipole interactions**

The electric field from a single point charge at a distance r from the charge is

$$E = kq/r^2 \quad . \tag{2.196}$$

The potential energy of a charge-dipole system is

$$U(r) = -\frac{k|q|}{r^2}\cos\theta \quad . \tag{2.197}$$

The potential energy now falls off as $1/r^2$, more rapidly than the charge-charge system. In the absence of thermal motion, the dipole will align with the $\mathbf{E}$ field, which corresponds to $\theta = 0$.

Because of random collisions with the molecules of the surrounding medium, the dipole will undergo a Brownian motion. Here we will consider only the change in the orientation of the dipole as a result of random collisions and write down the Boltzmann probability that the dipole makes an angle θ with the $\mathbf{E}$ field as

$$P(\theta) \propto \exp(-\beta U) = \exp(pE\beta\cos\theta) \tag{2.198}$$

The average value of the potential energy, averaged over all possible orientations whose probability is given by the Boltzmann distribution, can be written as

$$< U >= -\frac{1}{Z}\int_0^\pi d\theta pEcos\theta e^{pE\beta\cos\theta} 2\pi\sin\theta \quad , \tag{2.199}$$

where Z is the normalization constant. Solving this integral yields

$$< U >= -pE\left(\coth\left(\frac{pE}{k_BT}\right) - \frac{k_BT}{pE}\right) \tag{2.200}$$

which, in the limit $pU \ll k_BT$, simplifies to

$$< U >= -\frac{p^2 E^2}{3k_B T} \tag{2.201}$$

Substituting for the electric field due to a point charge q at a distance r from the charge, we get

$$< U >= -\frac{(kqp)^2}{3k_B T r^4} \tag{2.202}$$

With thermal averaging, the charge-dipole interaction falls off as $1/r^4$.

– **Dipole-dipole interactions**

The interaction energy of two permanent dipoles depends on their relative orientation, and might be expected to be zero overall for a compound if all orientations are possible. This would be true if the molecules were completely free to rotate, but they are not and some orientations are preferred over others.

Let $\mathbf{p}_1$ and $\mathbf{p}_2$ be two dipoles. The potential energy has the form

$$U(r) = -\mathbf{E}_1 \cdot \mathbf{p}_2 = k\frac{p_1 p_2}{r^3} F(\theta_1, \phi_1, \theta_2, \phi_2) \quad , \tag{2.203}$$

where $\mathbf{E}_1$ is the electric field from dipole $\mathbf{p}_1$and depends on the angular position of $\mathbf{p}_2$ relative to $\mathbf{p}_1$ and their relative orientations. The distance dependence 1/r3 comes from the radial dependence of the electric field $\mathbf{E}_1$ of dipole $\mathbf{p}_1$.

The thermal averaging with Boltzmann probabilities, in the limit $U \ll k_B T$, gives

$$< U >= -\frac{2}{3}\frac{(kp_1 p_2)^2}{3k_B T r^6} \quad . \tag{2.204}$$

Thus the potential energy between two dipoles falls off as $1/r^6$ power, i.e., dipole-dipole interactions are short-range interactions.

– **Van der Waals interactions**

Perhaps the most important class of dipole-dipole interactions are the ones where one or both molecules do not have a permanent dipole. These interactions are valid for any two atoms that come into close contact with each other, and are called Van der Waals interactions. .

* **Dipole-induced dipole interactions**
  A molecule with a permanent dipole $\mathbf{p}_1$ can induce a dipole in another polarizable molecule. In this case the induced dipole moment $\mathbf{p}_2^*$ points in the same direction as the inducing electric field $\mathbf{E}_1$. The potential energy of interaction between p_1 and p_2^* takes the form

$$U(r) = -\frac{kp_1p_2^*}{r^3}f(\theta) \tag{2.205}$$

  where the minus sign indicates that the interaction is always attractive, since the induced dipole always follows the direction of the instantaneous electric field. θ defines the angular position of $\mathbf{p}_2^*$ relative to $\mathbf{p}_1$ and the electric field $\mathbf{E}_1$ is independent of the azimuthal angle ϕ.
  The magnitude of $\mathbf{p}_2^*$ depends upon the strength of the electric field at position (r, θ)

$$p_2^* = \epsilon_0\alpha_2 E_1(r,\theta) = \epsilon_0\alpha_0\frac{kp_1}{r^3}f(\theta) \quad , \tag{2.206}$$

  where α_2 is the polarizability of the second molecule. The interaction potential is given by

$$U(r) = -\alpha_2\epsilon_0\frac{k^2p_1^2}{r^6}f^2(\theta) \quad , \tag{2.207}$$

  where again we have a $1/r^6$ dependence in the absence of thermal averaging. Hence averaging will also give the same contribution since we only need to average over the angle θ.
* **Induced dipole-induced dipole interactions**
  A fluctuating electric field environment around each atom induces a fluctuation dipole moment that is proportional to the polarizability of the atom. This instantaneous dipole can then induce a dipole in a neighbouring atom, resulting in an attractive potential that also has a $1/r^6$ dependence.
* **Short-range repulsive interaction**
  As the atoms get too close, at some point there is a strong repulsion from overlapping electron clouds and Pauli's exclusion

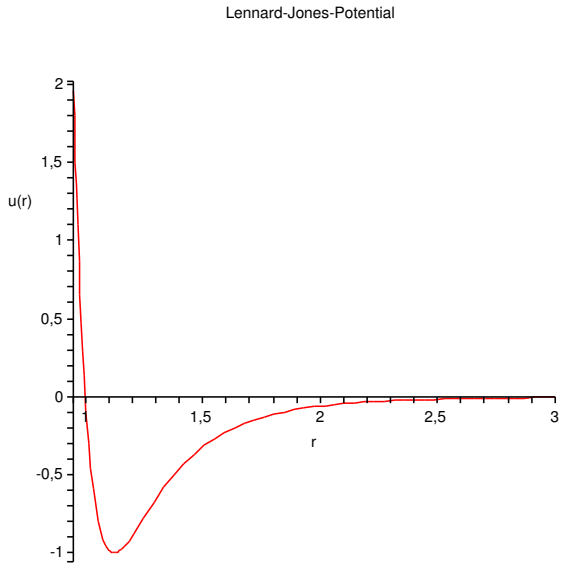

Figure 2.39: Lennard-Jones potential for the parameter $\sigma = 1$.

principle whereby filled electron shells of an atom cannot accommodate any more electrons.

* **Lennard-Jones potential**
  A commonly used analytical form that lumps together all dipole-dipole interactions and includes both the attractive and the repulsive terms is the Lennard-Jones potential, where the repulsive term is approximated as having a $1/r^{12}$ dependence

$$U_{\mathrm{LJ}}(r) = 4\epsilon \left[\left(\frac{r}{\sigma}\right)^{-12} - \left(\frac{r}{\sigma}\right)^{-6} \right] \quad . \tag{2.208}$$

  The atoms can be treated as spheres defined by a van der Waals radius that is a measure of how close another atoms can come before a strong, very short range, repulsive force kicks in.
  Some typical Van der Waals radii of atoms are hydrogen $1.2\mathring{A}$, oxygen $1.4\mathring{A}$, nitrogen $1.6\mathring{A}$, and carbon $2\mathring{A}$.

- **Hydrogen bonds**

  A very important interaction responsible for the structure and properties of

water, as well as the structure and properties of biological macromolecules, is the hydrogen bond. A hydrogen bond is an interaction between a proton donor group D-H and a proton acceptor atom A.

D-H is strongly polar, which means that the electron density is primarily around the electronegative atom (examples, F-H, O-H, N-H, S-H in order of decreasing polarity). The acceptor atom A is also strongly electronegative.

The hydrogen bond interaction is more than just an ionic or dipole-dipole interaction between the donor and the acceptor groups. The distance between the H and A in a hydrogen bond is less than the sum of their respective Van der Waals radii.

The strength of the hydrogen bonds in biological macromolecules ranges from $2k_BT$ to $5k_BT$.

- **Hydrophobic interactions**

  Another very important interaction is the hydrophobic interaction. As the term hydrophobic suggests, this interaction is an effective interaction between two nonpolar molecules that tend to avoid water and, as a result, prefer to cluster around each other.

  Unlike all the other interactions that we have studied so far and which are pairwise interactions between atoms or parts of molecules, the nature of the hydrophobic interaction is very different. It involves a considerable number of (water) molecules, and does not arise as a result of a direct force between the nonpolar molecules.

  Nonpolar molecules are not good acceptors of the hydrogen bond. When a nonpolar molecule is placed in water, the hydrogen bonding network of water is disrupted. The water molecules therefore reorganize around the solute and make a sort of cage, similar to the structure of water in ice, in order to gain back the broken hydrogen bonds. This reorganization results in a considerable loss in the configurational entropy of water and therefore an increase in the free energy G.

  If there are two or more such nonpolar molecules, the configuration in which they are spatially together (clustered together) is preferred because

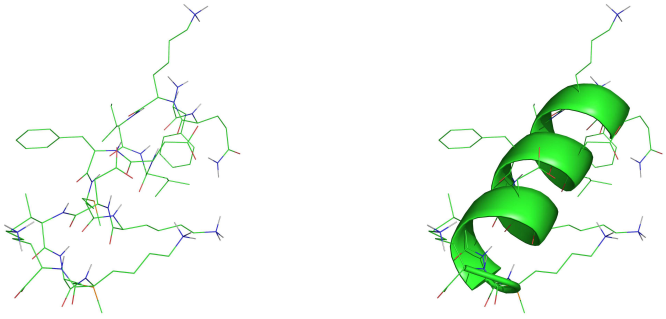

Figure 2.40: Helical structure found in polypeptides. To better identify the helical structure the right picture shows a cartoon of the helix.

now the hydrogen bonding network of water is disrupted in one (albeit bigger) pocket, rather than in several small pockets. Therefore, the entropy of water is larger when the nonpolar molecules are clustered together, leading to a decrease in the free energy.

At equilibrium, the configuration with the lower free energy and which has a higher Boltzmann probability, is the preferred configuration.

Hydrophobic interactions have strengths of a few k_BT and are comparable in energy to hydrogen bonds.

2.3 Helix-Coil Transition

The α-helix is the most abundant helical conformation found in globular proteins. In the α-helix the polypeptide folds by twisting into a right-handed screw, so that all the amino acids can form hydrogen bonds with each other. The helix has maximal intra-chain hydrogen bonding. This high amount of hydrogen bonding stabilises the structure so that it forms a very strong rod-like structure. The amino group of each AA residue is hydrogen bonded to the carboxyl group of the 4th following AA residue, which is on an adjacent turn of the helix.
Along the axis of the helix, it rises 0.15 nm per AA residue, and there are 3.6 residues/turn of the helix. This means, that AA residues spaced 4 apart in the

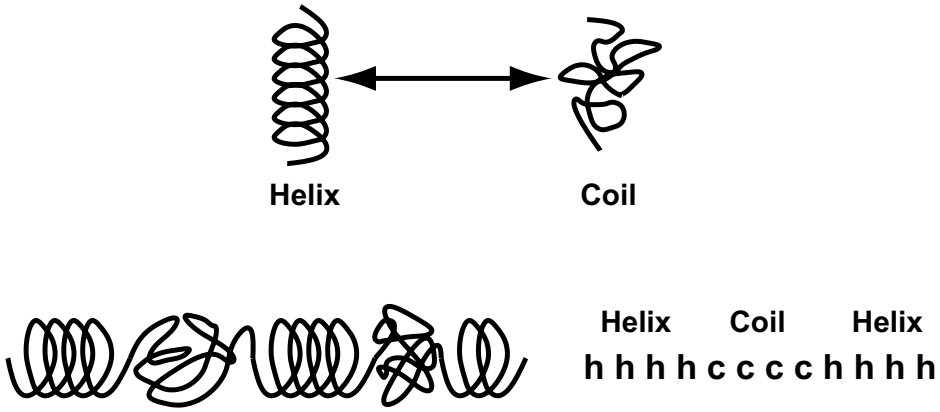

Figure 2.41: Mapping of the helix-coil transition onto a sequence of symbols

linear chain are quite close to one another in the α-helix. The screw-sense of any helix can be RH or LH, but the α-helix found in proteins is always RH. The average length of an alpha helix is about 10 residues.
What we want to consider now is that upon increasing the temperature, the helix structure goes over into a random coil structure [**?**, **?**, **?**].
To describe the macromolecule in terms of helical and non-helical parts, we denote by h a helical monomer and by c a coil monomer (see later for the analogy with the Ising model [**?**]). A conformation is then characterised by a sequence of h and c, which we denote by $\{h, c\}$. An example for such a sequence is

$$\cdots hhccchc\cdots \tag{2.209}$$

Since there are N monomers, we have 2^N states. To be able to write down a partition function, we assume that the energies of the h- and the c-sequence are independent and that they only depend on the length of the corresponding sequence. Then we can write down individual statistical weights

$$u_i = \exp\{-\beta E_i(c)\} \tag{2.210}$$

for the c-sequence with i coil-like connected monomers. Likewise for the helical sequence

$$v_i = \exp\{-\beta E_i(h)\} \quad . \tag{2.211}$$

Here we have implicitly assumed that the energy is independent of the position within the chain and independent of the neighbouring sequences! Also self-avoidance has been ignored, since we do not take into account that monomers may be linearly located far apart but may get in contact with each spatially. Given all these assumptions we write down the partition function

$$Z_N = \sum_{\{h,c\}} e^{-\beta E(\{h,c\})} \tag{2.212}$$

$$= \sum_{i,j} \prod_{i,j} u_i v_j \quad . \tag{2.213}$$

Everything hinges now on the distribution of the h- and the c-sequences. Let us write for the sequence $\{h, c\}$:

$$i_0, j_1, i_1, ..., j_M, i_M, j_0 \quad , \tag{2.214}$$

where i denotes the length of the c-sequence and j the length of the h-sequence. All $2M$ inner sequences contain at least one unit

$$M \leq \lfloor N/2 \rfloor \tag{2.215}$$

with the constraint

$$\sum_{k=0}^{M} (i_k + j_k) = N \quad . \tag{2.216}$$

Hence we can write

$$Z_N = \sum_{M=0}^{\lfloor N/2 \rfloor} \sum_{\{i_k, j_k\}} \prod_{k=0}^{M} u_{i_k} v_{j_k} \quad . \tag{2.217}$$

From the preceding section it is clear, that if we consider very long chains ($N \to \infty$) then the free-energy will be proportional to N, i.e., chain end effects will not play any role

$$Z_N \approx q_{\text{eff}}^N \quad \text{for} \quad N \gg 1 \quad , \tag{2.218}$$

where q_{eff} is the average contribution per monomer to the free-energy.

Let us now look at the generating function

$$\Gamma(x) = \sum_{N=0}^{\infty} Z_N x^{-N} \quad . \tag{2.219}$$

This series converges for $x > q_{\text{eff}}$ and diverges for $x \to q_{\text{eff}}$

$$\Gamma(x) \quad < \quad \infty \quad x > q_{\text{eff}} \tag{2.220}$$

$$1/\Gamma(x) \quad = \quad 0 \quad x = q_{\text{eff}} \quad . \tag{2.221}$$

Hence the partition function is the largest root of eq **??**. So, let us look at the Γ in more detail

$$\Gamma(x) \quad = \quad \sum_{N=0}^{\infty} x^{-N} \sum_{M=0}^{\lfloor N/2 \rfloor} \sum_{\{i_k, j_k\}} \prod_{k=0}^{M} u_{i_k} v_{j_k} \tag{2.222}$$

$$= \quad \sum_{M=0}^{\infty} \sum_{N=2M}^{\infty} \sum_{\{i_k, j_k\}} \prod_{k=0}^{M} u_{i_k} x^{-i_k} v_{j_k} x^{-j_k} \tag{2.223}$$

$$= \quad \sum_{M=0}^{\infty} \sum_{i_0=0}^{\infty} \frac{u_{i_0}}{x^{i_0}} \sum_{j_0=0}^{\infty} \frac{v_{j_0}}{x^{j_0}} \prod_{k=1}^{M} \sum_{i_k=0}^{\infty} \frac{u_{i_k}}{x^{i_k}} \sum_{j_k=0}^{\infty} \frac{v_{j_k}}{x^{j_k}} \quad . \tag{2.224}$$

The sums over i_k and j_k do not depend on k any more. Only the ends can have a different weight. For $k \geq 1$ we can define

$$U(x) \quad \equiv \quad \sum_{i=1}^{\infty} u_i x^{-i} \tag{2.225}$$

$$V(x) \quad \equiv \quad \sum_{j=1}^{\infty} v_j x^{-j} \tag{2.226}$$

which converge in $q_{\text{eff}} < x < \infty$, since $\Gamma(x)$ converges. With this we have

$$\Gamma(x) \quad = \quad U_0 V_0 \sum_{k=0}^{\infty} (UV)^k \tag{2.227}$$

$$= \quad U_0 V_0 \frac{1}{1 - UV} \quad . \tag{2.228}$$

$\Gamma(x), U(x)$ and $V(x)$ are positive and monotone decreasing functions of x since the statistical weights are positive and real. It follows that $1/\Gamma(x)$ is a continuous and monotonically decreasing function in $q_{\text{eff}} < x < \infty$, since $\Gamma(x)$ and $1/\Gamma(x) = 0$ for $x = q_{\text{eff}}$. Since

$$U_0 V_0|_{x=q_{\text{eff}}} \neq 0 \tag{2.229}$$

we have

$$U(q_{\text{eff}})V(q_{\text{eff}}) = 1 \quad . \tag{2.230}$$

In a chain composed of six units only four contribute with hydrogen bonds to the helical structure. In general, we have that for j consecutive helical states only $(j-2)$ are formed by hydrogen bonds. Hence we need three states in our model:

- a coil-like state
- a helical state with hydrogen bond.
- a helical state without hydrogen bond,

Corresponding to these three states we need statistical weights

$$\text{coil} \quad - \quad u \tag{2.231}$$

$$\text{h} \quad \text{with} \quad \text{h}-\text{bond} \quad - \quad v \tag{2.232}$$

$$\text{h} \quad \text{without} \quad \text{h}-\text{bond} \quad - \quad w \tag{2.233}$$

If we take as a reference the coil state then we have the weights

$$\text{coil} \quad - \quad u/u = 1 \tag{2.234}$$

$$\text{helix} \quad \text{with} \quad \text{h}-\text{bond} \quad - \quad w/u = s \tag{2.235}$$

$$\text{helix} \quad \text{without} \quad \text{h}-\text{bond} \quad - \quad v/u = \sigma^{1/2} \tag{2.236}$$

For the sequences of h and c we get

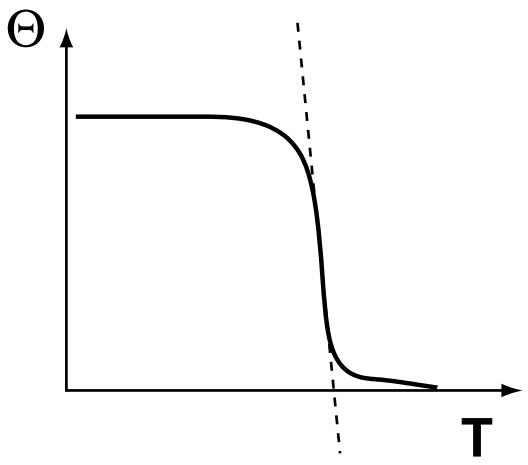

Figure 2.42: Dependence of the order parameter on the temperature for the helix-coil transition

$$\begin{array}{cccc} c-\text{sequence} & & u_i = u^i & 1 \\ h-\text{with} & \text{h}-\text{bond} & v_j = v^2 w^{j-2} & v_j = \sigma s^{j-2} \\ h-\text{without} & \text{h}-\text{bond} & v_1 = v & v_1 = \sigma^{1/2} \end{array} \tag{2.237}$$

From the experimental point of view one can determine the relative number of unbroken hydrogen bonds θ (which is proportional to the number of w statistical weights).
With the above defined statistical weights and using eq **??** we have

$$Z_N = \sum_{ij} \prod_{ij} u_i v_j = \sum_{ij} \prod_{ij} \sigma s^{j-2} \tag{2.238}$$

We obtain θ by taking the derivative with respect to s

$$\theta = \frac{1}{N-2} \frac{\partial \ln Z_N}{\partial \ln s} \quad . \tag{2.239}$$

Since $Z_N \propto q_{\text{eff}}^N$ for $N \gg 1$ we find

$$\theta = \frac{1}{N} \frac{\partial \ln q_{\text{eff}}^N}{\partial \ln s} = \frac{s}{q_{\text{eff}}} \frac{\partial q_{\text{eff}}}{\partial s} \quad . \tag{2.240}$$

We determine q_{eff} from eq **??**

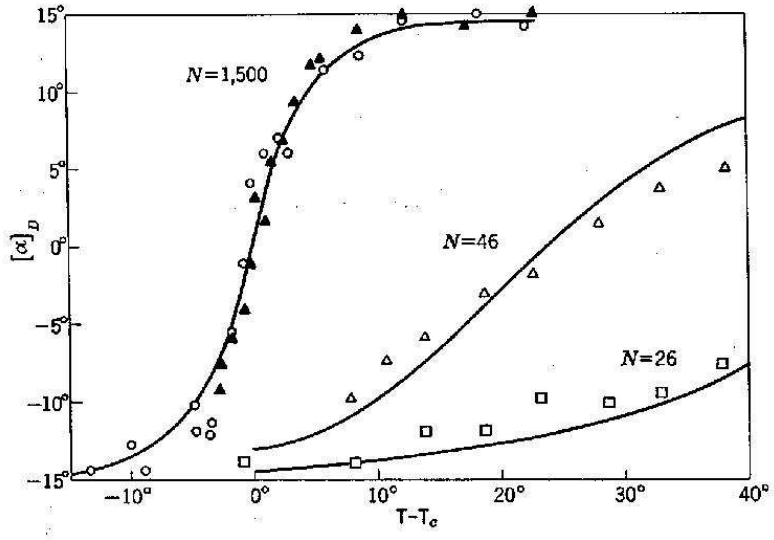

Figure 2.43: Experimental results for the helix-coil transition

$$q_{\text{eff}}^3 - q_{\text{eff}}^2(u+w) + q_{\text{eff}}(wu - uv) + uvw + v^2 u = 0 \tag{2.241}$$

with the solution

$$q_{\text{eff}} = \frac{1}{2}\left\{w + u + \sqrt{(w-u)^2 + 4uv^2/w}\right\} \tag{2.242}$$

and for θ

$$\theta = \frac{1}{2}\left\{1 + \frac{s-1}{\sqrt{(s-1)^2 + 4\sigma s}}\right\} \quad . \tag{2.243}$$

In figure **??** is shown the qualitative result for the order parameter θ. A comparison to the experimental findings is shown in figure **??**.
We can make contact with the Ising model by setting

$$\sigma = e^{-4J/k_B T} \tag{2.244}$$

$$s = e^{2H/k_B T} \tag{2.245}$$

to find

$$\theta = \frac{1}{2}\left\{1 + \frac{\sinh(H/k_BT)}{\sqrt{\sinh^2(H/k_BT) + e^{-4J/k_BT}}}\right\} \quad . \tag{2.246}$$

Hence the average magnetization per spin $< m >$ can be looked upon as the helical fraction

$$< m >= 2\theta - 1 = \frac{\sinh(H/k_BT)}{\sqrt{\sinh^2(H/k_BT) + e^{-4J/k_BT}}} \quad . \tag{2.247}$$

In this context the Ising model appears as a special case of the α-helix model.

2.4 DNA Melting

DNA melting refers to the dissociation of the two strands of the double helix by an increase of temperature. The melting is thus a highly cooperative thermal disruption of the hydrogen bonds between complementary bases in the double helix. At the equilibrium melting temperature half of the bonds are disrupted. Dissociation can occur also through a change of pH.
The melting or denaturation of DNA is a thermodynamic reversible phase transition. The order of the transition is still debated due to the effect to the entropy of loops embedded in the chain. Existing experimental studies of the thermal denaturation of DNA yield sharp steps in the melting curve suggesting, that the melting transition is first order. Here we present the Poland-Scheraga-model [**?**] and the zipper-model [**?**].
The Poland-Scheraga-model considers the DNA molecule as composed of an alternating sequence of bound and denaturated states as depicted in figure **??**. Consider two strands, made of up monomers, each representing one persistence length of a single strand. Typically a bound state is energetically favored over an unbound one, while a denaturated segment or loop is entropically favored over a bound one. Within the Poland-Scheraga-model the segments that compose the chain are assumed to be non-interacting with one another, i.e. excluded volume effects are not taken into account. This assumption considerably simplifies the theoretical treatment and enables one to calculate the resulting free energy.